Energy Conversion and Management: X 30 (2026) 101582

Contents lists available at ScienceDirect

Energy Conversion and Management: X

journal homepage: www.sciencedirect.com/journal/energy-conversion-and-management-x

Energy transition buildings: A representative case study of refurbished single household shifted to full electric utilities combined with PV, wind and battery storage

Claudio Zuffi, Daniele Fiaschi *

Department of Industrial Engineering (DIEF), University of Florence, Florence, Italy

A R T I C L E I N F O

Keywords:
Building energy transition
Dynamic analysis
Photovoltaics
Wind turbine
Battery energy storage
Rarity assessment

A B S T R A C T

The objective of the paper is a comprehensive energy and material rarity analysis of a representative example of household shifted to fully electric utilities, supported by uncommon combination of photovoltaic and wind renewables, complemented by battery storage. The manuscript provides figures of optimal battery storage sizing, complementarity of PV and wind resource and material rarity impact assessment, in a combined manner unavailable in literature. The approach and the considered example are generalizable to the wide category of single households and/or accommodation facilities in suburban areas, the countryside, the mountains and holiday resorts.

The manuscript analyses the dynamic behaviour of a moderately refurbished single-family household located in a country/suburban area of central Italy, grid-connected and fully electrified through a heat pump combined with Photovoltaics, Wind Turbine (PV/WT), and a Battery Energy Storage System (BESS). A dynamic model based on 12 representative monthly days was developed to evaluate the seasonal thermal and electrical behaviour of the building. It was validated against measured PV/BESS data from an existing case study, characterized by its overall pre-/post-refurbishment transmittance U. To avoid costly and invasive masonry interventions, the existing high-temperature heaters were preserved, and a high-temperature Heat Pump (HP) was adopted. The seasonal simulations enabled the optimization of the Battery Ratio (BR), defined as the BESS-to-(PV+WT) size ratio, to maximize the renewable fraction (Fr). Depending on the configuration, Fr ranged between 58.5 % and 65.6 % without WT, and increased up to 76.4–87.9 % with WT. The daily deficit associated with a PV string anomaly was quantified at 1–4 kWh under clear-sky summer conditions.

Finally, an element rarity (TR) assessment was carried out for HP, PV, WT, and BESS as a complement to standard sustainability metrics. The analysis highlighted a TR impact of 68.2 GJ for WT, 36 GJ for PV, and 21.3 MJ for HP, while a 7 kWh BESS reached 36.6 GJ, largely driven by cobalt (79.2 %).

This study provides a comprehensive example of household energy transition, combining moderate and cost-effective refurbishment strategies with an uncommon PV/WT integration, relying on data from a real case study. It also introduces material rarity as an additional sustainability indicator, with the aim of supporting more balanced design choices in the residential energy sector.

1. Introduction

The residential sector shares about 22 % of Total Final Consumption (TFC) of primary energy at global level, contributing to about 2 Gt CO_2 emissions per year. Within the EU27, this share rises to almost 25 %, corresponding to 303 Mt CO_2 per year [1]. The Paris Agreement (COP21) set a global roadmap to mitigate climate change, recognizing the building stock as a crucial sector due to its significant untapped efficiency potential [2]. In recent years, enhancing building energy efficiency has become increasingly relevant to achieving both short-term (2030) and long-term (2050) emission reduction targets [3]. To support this transition, most EU countries have introduced a range of incentive schemes, from conventional subsidies, tax benefits, and loans to more innovative mechanisms such as property tax reductions, on-bill financing, green mortgages, and energy efficiency feed-in tariffs [3]. Regulatory frameworks play a decisive role in shaping household investment choices, thereby influencing actual energy savings and CO_2

* Corresponding author.
E-mail address: Daniele.fiaschi@unifi.it (D. Fiaschi).

https://doi.org/10.1016/j.ecmx.2026.101582
Received 1 June 2025; Received in revised form 4 November 2025; Accepted 15 January 2026
Available online 17 January 2026

Nomenclature

Acronyms/Subscripts

BESS	Batteries Energy Storage System
BL	Baseload
BOS	Balance Of System
COP	Coefficient Of Performance
DHW	Domestic Hot Water
HP	Heat Pump
HC	Heating Cooling
MPP	Maximum Power Point
NOCT	Nominal Operating Cell temperature
OC	Open Circuit
PV	Photovoltaic
SC	Short Circuit
SOC	battery State Of Charge [%]
STC	Standard Test Conditions
TR	Thermodynamic Rarity
WT	Wind Turbine
i	Hourly values
day	daily values

Symbols

A	Surface Area [m^2]
α_{ISC}	coefficient of Short Circuit temperature [%/°C]
BR	Batteries/(PV+WT) size ratio [h]
β_{VOC}	coefficient of Short Circuit temperature [%/°C]
E	Generated Electricity (PV, WT, BESS) [kWh]
$E_{battery}$	Battery nominal size [kWh]
EL_{grid}	Electricity consumption from grid [kWh]
η	Efficiency [%]
Fr	Renewable Fraction
G_T	Solar radiation on tilted surface [W/m^2]
I	Current [A]
T	temperature [C]
U	Overall heat transfer coefficient [W/(m^2 K)]
V	Voltage [V]
W	Power [W]

mitigation outcomes [4].

The shift to electric utilities integrated with PV is, nowadays, among the most common ways in building energy transition. Several authors have addressed these issues, focusing on topics such as the role of demand profiles in the design of photovoltaic systems [5]; the integration of heat pumps, solar thermal, photovoltaic, and battery storage for residential applications [6]; the optimization of photovoltaic–battery system performance [7]; and the evolution of energy demand during the transition from gas heating to heat pumps [8]. Although the integration of heating and cooling systems compliant with European standards is relatively straightforward in new buildings, retrofitting existing ones remains more challenging and often economically unfeasible, even with public incentives.

A typical case is floor heating, widely recommended when adopting low-temperature heat pumps, which require low supply temperatures to achieve high seasonal COP values. However, with conventional air-to-water heat pumps, existing radiators are often undersized, and replacement with larger low-temperature floor heating systems is required to meet winter heating demand. Such interventions are usually invasive, involving extensive masonry works, and therefore neither cost-effective nor easy to implement. Moreover, system performance strongly depends on building type and flooring conditions. Vadiee et al. (2020) [9], in a comparison between radiator and floor heating systems in a single-family house, showed that building efficiency and construction type significantly affect heat demand and transmission losses. Their findings suggest that maintaining existing radiators, combined with modest refurbishments and/or the adoption of high-temperature heat pumps, often represents the most practical and affordable option.

The present work deals with the implementation of the heat pump in traditional heating systems with high-temperature radiators, assisted by a newly installed ducted fan coil unit into a moderately refurbished single-family household. The fan coil unit, where possible, with a simple lowering of the ceiling allows the heat pump to be used for summer cooling as well. This heating/cooling system, is suitably supplemented by a photovoltaic plant (PV) and a Wind Turbine (WT), working in synergy, combined with Battery Energy Storage System (BESS) sized in relation to the size of the PV and WT in such a way as to maximise the fraction of the electrical load of the utilities covered by the PV + WT + BESS system.

Several gaps emerge from the literature, which this work aims to address. The first concerns the limited attention given to family households, which typically have configurations that allow for substantial integration of renewable energy sources, such as PV and WT. Some statistical analyses confirm the relevance of this building category: within the EU in 2023, 51.7 % of the population lived in houses, while 47.7 % lived in flats. Houses, including terraced ones, are most common in two-thirds of EU countries, with shares varying by country and urban vs. rural setting. In Italy, about 41.2 % of people lived in independent or semi-independent households [10]. These homes are generally larger and more energy-consuming than flats. Therefore, upgrading their heating/cooling systems and integrating renewables can significantly support the building energy transition. Additionally, single-family homes typically have larger rooftop areas per occupant for PV installation.

Despite their relevance and the interest in energy transition, these buildings are only marginally covered in the scientific literature on energy efficiency measures. Case studies with measured data and modeling are also rare and they are as follow. Mulleriyawage and Shen (2020) [11] analyzed the optimal sizing of a battery-PV system for a household in Victoria, Australia. Chhugani et al. (2023) [12] compared different heating systems for a single-family home, focusing on PVT and heat pump systems. Baraskar et al. (2023) [7] evaluated a controlled PV-HP-battery system in a single-family household in Germany, suitable for integration into a smart grid. Terry and Galvin (2023) [8] examined changes in heat demand and energy consumption in households transitioning from gas boilers to heat pumps, referring to a UK household. Olympios et al. (2022) [13] proposed operational optimization of an air-source heat pump system for space heating and domestic hot water in a single-family dwelling, developing comprehensive thermal network models for both a standard configuration and an advanced setup with phase-change material thermal storage.

The second gap evident in the literature is that while considerable attention is given to resources such as PV systems and batteries, the adoption of small WT is seldom addressed due to legal, aesthetic, and social barriers. This issue becomes particularly relevant for single-family, suburban, or rural homes, as well as tourist resorts, which often have sufficient outdoor space to accommodate small WT. In 2006, Hessami [14] proposed the design of a hybrid wind and solar energy supply system for a rural residential building with PV coupled to a 2.5 kW wind turbine. In 2015, González et al. [15] presented an optimization methodology for minimum life cycle cost of a grid connected Hybrid PV, wind and biomass power. In 2017, Hajdidj et al. [16] evaluated an optimized system for producing electricity from one or two renewable energy (like solar and wind) in a low wind potential site for autonomous dwellings. In 2018, Giallanza et al. [17] proposed the sizing of a stand-alone hybrid PV/WT/BESS system applied to a Sicilian case study. In

2019, Ramirez Camargo et al [18] analysed the potential of hybrid renewable energy systems for self-sufficient residential use in Germany and the Czech Republic. In 2020, Rehman et al. [19] analysed an optimal hybrid power system based on wind, solar, diesel, and battery backup, capable of addressing the load requirements of an Indian village. Drozd and Kowalik, in 2021 [20] presented a technical comparison of PV and a wind farm for powering a residential single-family building. In 2021, Nguyen and Boström [21] proposed a multi-objective optimization of a hybrid wind/solar battery energy system in the Arctic region of Tromsø, Norway.

The third gap is that the literature rarely considers the impact of critical materials in the energy performance and environmental assessment of buildings retrofitted with renewable energy systems, like PV and wind turbines, supported by BESS. The shift of buildings towards fully electric utilities supported by variable renewable energy (VRE) and battery energy storage systems (BESS) relies heavily on technologies containing critical materials. Batteries, in particular, involve elements with high environmental and energy impacts, and some are sourced from scarce natural resources, potentially affecting the sustainability of these solutions. McManus (2012) [22] assessed the energy, material, and greenhouse gas impacts of various battery types, while Grandell et al. (2016) [23] identified the most critical elements for future clean energy technologies e.g. silver, tellurium, indium, dysprosium, lanthanum, cobalt, platinum, and ruthenium. More recently, Huber and Steininger (2022) [24] highlighted social, economic, and conflict-related issues associated with tin (PV panels), rare earth elements such as praseodymium, dysprosium, neodymium (wind turbine magnets), lithium, and cobalt (Li-ion batteries). Specifically, there is a lack of studies evaluating the rarity and sustainability implications of introducing these technologies in residential households, representing a clear gap covered by the current research.

The main objective of this paper is to propose moderate yet affordable strategies for building energy transition, based on zero to moderate refurbishment combined with a flexibly sized PV/WT/BESS system. This approach allows different options to achieve significant renewable energy coverage of household loads. The analysis focuses on a single-family home in a suburban or rural area of central Italy, with modest but non-negligible wind resources. This study serves as a starting point for generalization to a broader range of similar buildings, potentially including small touristic structures. Here, a measure of drawbacks related to the building's energy transition in terms of impact on critical elements is proposed by analysing the rarity introduced by the HP/PV/WT/BESS equipment, which may be also useful in adjusting the sizing and relative proportions of different possible renewables and BESS size. This kind of assessment is not available in the literature referred to building's energy transition, where the improvements are generally expressed in terms of reduction of energy consumption and carbon footprint.

Summarizing, this paper explores at least four key aspects that are either scarcely addressed in the scientific literature, highlighting both the novelty of the study and its potential to give a significant contribution to the field:

1. The analysis of a relevant category of households in Europe and worldwide, subjected to a feasibly moderate level of refurbishment, combined with PV/WT renewable energy and BESS in the framework of operations for building energy transition.
2. The modelling validation against a real case study, representative of the selected building category, which data are seldom available in literature and afterwards become also useful to assess possible working anomalies of the energy system.
3. Compared to more complex modelling and tools proposed in literature, this one is particularly suitable for educational purposes, allowing a smooth yet effective interpretation of the physical reasons behind the choice of moderate affordable choices in building refurbishing.
4. The addition and evaluation, to the traditional PV, of a suitable WT in an area with modest wind resource to assess its contribution to the renewable fraction used to cover the building electric loads.
5. The rarity assessment of the building energy transition, highlighting the criticality of the main involved technological components like HP, PV, WT, BESS as an important complement to the traditional ones in defining the sustainability of the interventions, such as the carbon footprint.

2. Methodology

This section is divided in three main sub sections. Section 2.1 is dedicated to the dynamic modelling framework of the PV–wind–BESS system coupled with building heating, cooling, and baseload, including the calculation of building electric loads (Section 2.1.1), the simulation of renewable generation and storage (Sections 2.1.2–2.1.3), and the hourly control logic for battery operation (Section 2.1.4). Section 2.2 presents the representative case study, detailing the improvements of refurbished building envelope, heat pump and PV–battery integration, validated baseload profiles, and indoor setpoints for calculating the dynamic hourly COP and electricity consumption. Finally, Section 2.3 introduces the Thermodynamic Rarity indicator, which assesses the material scarcity of energy system components using an exergy-based approach.

2.1. Dynamic model of PV/WIND/BESS/grid coupled to building utilities and baseload

The main purpose of the developed model is realizing a not very complex but effective tool for the dynamic simulation of the building – heat pump/chilling – PV/WT/BESS grid connected system, suitable for the analysis of energy needs and the sensitivity of the performance to the BESS/PV-WT size ratio. The model is particularly suitable for single family household's category and suburban, countryside, seaside and hill/mountain small touristic resorts. The model has an academic root, originally developed for the course of Renewable Energy and subsequently evolved towards research features. It is structured to be easily applicable to different household types and different buildings categories, also including industrial and service ones. The main constraint of the model is the need of the system components' data: building and its heating/cooling devices, heat pump/chiller and PV/WT/BESS characteristics. They often rely on manufacturers' data, which are not always reliable and require a certain degree of experience from the operator, additionally to an accurate check. On the other hand, this approach makes the simulation model open to get always improved data of components as input, including those coming from experimental campaigns or from more accurate models, thus keeping the calculations open to updates and improvements. Finally, the seasonal dynamic based on the average monthly representative day makes the model unsuitable for implementation with weather forecast, load prediction, peakload shaving and optimization of BESS charge/discharge time. The schematic of the building/utility system served by PV/WT/BESS/GRID is sketched on Fig. 1. The main components are the PV/WT renewable electricity generation system, the inverter, the BESS, the electric load (including baseload and HP) and the grid connection through the Grid exchange meter.

2.1.1. Modelling building utilities to calculate the total electric load

The dynamic building load model is based on a monthly representative day, during which heating, cooling, and Domestic Hot Water (DHW) demands are calculated. These are converted into electrical loads using heat pump/chiller (HP) performance data and combined with the baseload (BL) from appliances, lighting, and other utilities. The total hourly electricity demand of the building is therefore the sum of HP demand for space heating/cooling $W_{HP_{HC_i}}$, the DHW W_{HPDHW_i} and the BL W_{BLi}, as reported in equation (1). The subscript "i" denotes the hourly

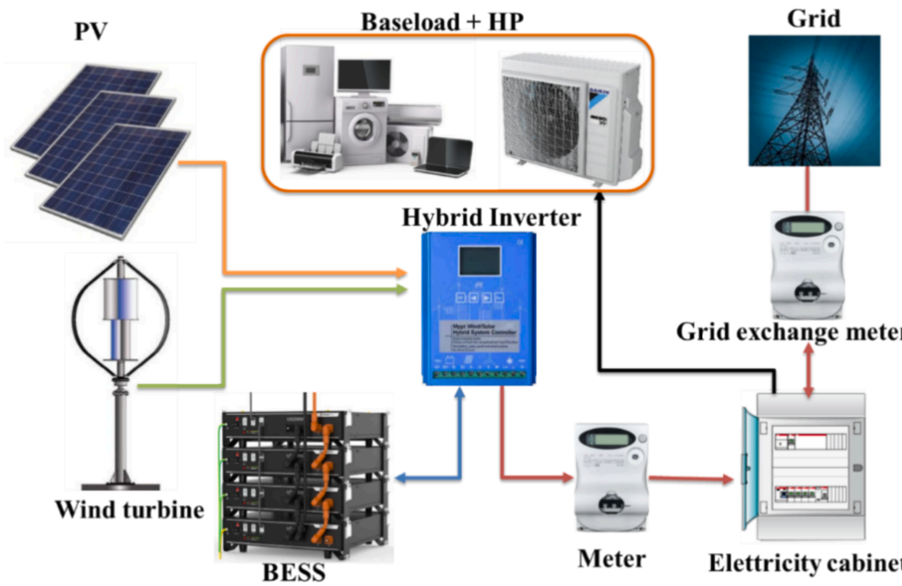

Fig. 1. Schematic of the building/utility system equipped with PVWT/BESS and basic electricity loads.

values, defining the time dependence in all equations. While the formulas themselves are not strictly dynamic, considering all hourly terms together provides a dynamic profile of the system's behaviour over time.

$$W_{TOT\,month\,i} = W_{HP_{HC_i}} + W_{HPDHW_i} + W_{BLi} \quad (1)$$

The model is divided in two sections:

1. The first estimates the total dynamic electricity demand of household utilities.
2. The second uses this demand as input to calculate the dynamic balance of the PV/WT/BESS/Grid system.

The schematic of the first part of the modelling code workflow for the calculation of the hourly heat pump/chiller electric load (**$W_{HP\ HCi}$**) is shown on Fig. 2. This load depends on three data series:

1. ***Building data***, based on the analysis of the building's heating and cooling demand, which depends on its geometry, architectural features, and envelope characteristics. For modelling purposes, the building is synthetically represented by the overall heat transfer coefficient U expressed as the UA product, including air exchange, where A is the total envelope surface area. It can be derived from the building's energy characterization. The data refer to a real case study of a single-family house that has undergone moderate refurbishment and has been converted to electric utilities integrated with PV and a battery system. This case is described in detail in the following chapter, which illustrates the application of this part of the model.
2. ***Daily hourly temperature profiles*** indoor ($T_{ID,i}$) and outdoor ($T_{amb,i}$). $T_{amb,i}$ seasonally defined by the average monthly representative day, achieved from local meteorological station data. This representative day is obtained from hourly averages of the available 15-minute data collected across all days of the selected month.
3. ***Heating/cooling system data***: depending on the characteristics of the system and the outdoor conditions, the required temperature from the heat pump/chiller is calculated.

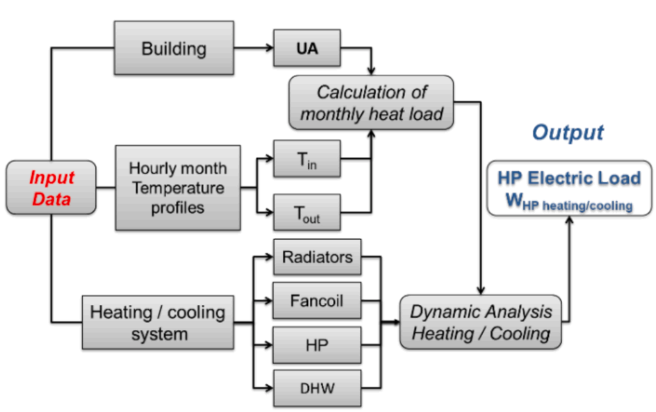

Fig. 2. Building/heaters/Heatpump system modelling code workflow.

On this basis, the hourly seasonal COP of the machine is determined and, from the building heating/cooling load, the dynamic **$W_{HP\ HCi}$** is calculated.

The terminal heaters and coolers of the building (e.g. radiators, fan coils, floor heating) represent a pivotal part of the dynamic modelling, determining the temperature required from the heat pump/chillers, the related hourly COP and thus the electricity demand. Hydronic heaters are considered here. The nominal heating power (size) is defined by the heaters surface area, which is an input data to the model, retrieved from radiators design data. As the analysis is referred to a building pre and post moderate refurbishment, the existing heating system is considered unchanged, thus characterized by the nominal installed size of the radiators, referred to their nominal working conditions (Table 1).

The nominal heating power (Q_{NOM}) is referred to ΔT_{NOM}. The heat output of the hydronic radiators is calculated here with equations (2) and (3) according EN 442 rule [25,26], largely adopted to standardize the heating systems in the EU. Accordingly, the nominal heat emission is determined in a room test with ΔT_{NOM}. Under the actual conditions of

Table 1
Nominal characteristics of the household radiators heating system.

Parameter	Amount	Unit	Description
$T_{in\,NOM}$	75	°C	nominal heaters water inlet Temperature
$T_{out\,NOM}$	65	°C	nominal heaters water outlet Temperature
T_{ID}	20	°C	Nominal temperature design
ΔT_{NOM}	50	°C	difference between the average of T_{NOM} and T_{ID}
ϵ	1.33	–	heaters characteristic exponent (radiators)
η_e	0.97	–	Radiators heat transfer efficiency
η_R	0.98	–	control system efficiency
η_D	0.97	–	distribution efficiency

use, the heat emission varies with this temperature difference, according to the scheme in Fig. 3a.

$$q_i = q_{NOM}\left(\frac{\Delta T_i}{\Delta T_{NOM}}\right)^{\varepsilon} \quad (2)$$

$$\Delta T_i = T_{mi} - T_{IDi} = \frac{T_{ini} + T_{outi}}{2} - T_{IDi} \quad (3)$$

ΔT_i is the actual difference between the radiator mean temperature T_{mi} and the indoor temperature T_{IDi} under conditions different from the nominal.

The heaters are generally designed for the most critical conditions, and in a large fraction of heating season the required heating power to maintain the indoor comfort temperature, as defined T_{ID}, is significantly lower than the design value. For this reason, to maximize the COP, the heat pump operation mode is determined by the real hourly heating demand, as evaluated in equation (4).

$$Q_{Hi} = U \bullet A \bullet (T_{ID} - T_{amb,i}) \quad (4)$$

In different seasons and times with variable $T_{amb\ i}$, the heating load Q_i is variable, thus different $T_{in\ i}$ are required. For this reason, the heat pump can work at the minimum required temperature to match the building heating demand Q_i, thus maximizing the COP_i. The minimum required radiators inlet temperature $T_{in\ i}$ is determined, hour by hour, calculating the required ΔT_i from equation (2) to balance the heat demand with the n installed radiators evaluated in equation (5).

$$Q_{Hi} = n \bullet q_i \quad (5)$$

Finally, equation (3) determines $T_{in\ i}$. The in/out radiators temperature difference $T_{in\ i} - T_{out\ i}$ is defined by the radiators design, generally 10 °C as assumed here. This approach considers the building and the heating/cooling system as a whole (single room), characterized by the overall averaged transmittance U, which is enough to the main goal of this work, not focused on a detailed assessment of the building. The calculation model also includes the hourly summer cooling load and, through the COP of the reversed air/water heat pump, the related electricity consumption. Here, a fan coils system with internal air/water heat transfer units equipped with ducted air fans is considered and referred to the schematic in Fig. 3b. These units may be used also in heating mode. In summer cooling mode, the cooling water temperature into the fan coil circuit is set within the 7 – 12 °C range.

Through the heat exchanger unit, the cooling power $Q_{C,fancoil}$ is transferred from the air to the water. As a result, a decrease in air temperature and an increase in water temperature are achieved. This is evaluated in equation (6) of the system in Fig. 3b.

$$Q_{C,fancoil} = \dot{m}_{air} c_{p,air} \Delta T_{air} = \dot{m}_{H2O} c_{p,H2O} \Delta T_{H2O} \quad (6)$$

Where m_{air} is the fan coil air flowrate (characteristic of the machine sized to match the building needs under the most critical operating conditions), c_{pair} and c_{pH2O} are the air and water specific heats, ΔT_{air} is the air temperature drop through the heat exchanger unit and ΔT_{H2O} is the water temperature rise through the heat exchanger unit.

The seasonal summer cooling is referred to Italy, so typically from May to September. The condition for activating the cooling is suitably referred to UNI 10339 normative (AICARR, 2008) [26], considering conventionally positive the heat flow from indoor to outdoor direction: $T_{ID\ i} \geq 26$ °C (UNI 10339) and $Q_{Ci} < 0$.

Under these conditions, the balance between the cooling load and the fan coil heat exchanger allows calculating the water flowrate and air outlet temperature. With the outdoor temperature and the design water range (7/12 °C), the COP_{Ci} and the cooling electricity demand are determined.

The hourly Domestic Hot Water load (DHW) is estimated using UNI 9182 data for average demand and storage sizing (needed to keep COP reasonable at 40–60 °C). The hourly demand is based on typical daily profiles [27], and the required heat input $Q_{DHW\ i}$ is given by equation (7).

$$Q_{DHW\ i} = m_{DHWi} \cdot c_{pH2O} \cdot (T_{DHW} - T_{Wi}) \quad (7)$$

where T_{DHW} is the required temperature of DHW and T_{Wi} is the water temperature inlet from waterworks, fixed or seasonally variable if available.

Finally, to determine the hourly electricity demand of the heat pump to supply the heating/cooling and DHW heat loads, the manufacturer's data of COP vs heating/cooling water temperature and environmental temperature (COP_{DHWi}) are used in equations (8), (9) and (10).

$$W_{HP_{heatingi}} = \frac{Q_{Hi}}{COP_{Hi}} \quad (8)$$

$$W_{HP_{coolingi}} = \frac{Q_{Ci}}{COP_{Ci}} \quad (9)$$

$$W_{HP_{DHWi}} = \frac{Q_{DHWi}}{COP_{DHWi}} \quad (10)$$

2.1.2. Dynamic modelling of PV/wind/battery/grid system (PV/WT/BESS/Grid)

The second part of the modelling code allows the dynamic analysis of the PV/WT/BESS/Grid system shown in Fig. 1 to cover the above calculated electric loads, which are taken as inputs. The schematic flowchart of this part of the calculation model is shown in Fig. 4. Coupling the local data of wind, solar radiation and temperature with those of the PV/WT/BESS system, the code provides the daily dynamic behaviour of produced electricity, self-consumption, battery State Of Charge (SOC) and grid electricity exchange.

The objective is to analyse the hourly and seasonal behaviour of renewable energy from PV and wind turbine in support of the household electric load, while harmonizing BESS and PV/WT sizing with respect to the available household roof and/or surrounding surface area. The calculation model can also be used to optimize PV/BESS sizing, aiming to maximize the solar fraction and/or minimize household electricity

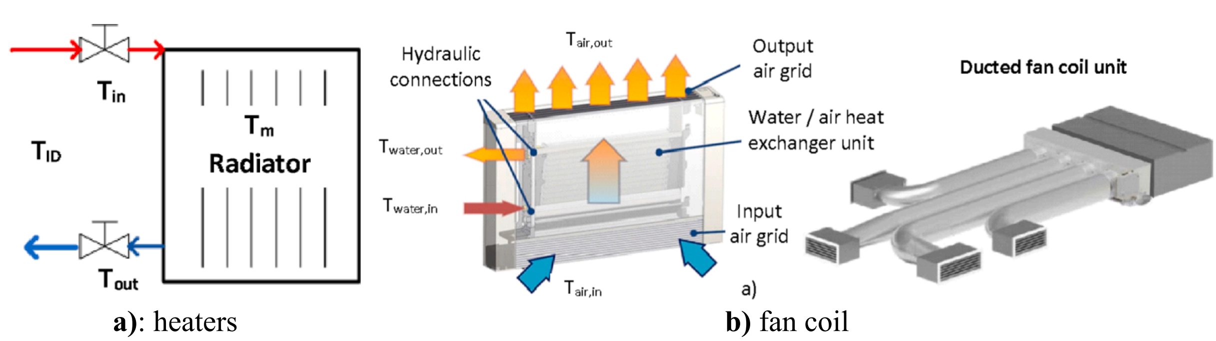

Fig. 3. Schematic of heaters and fan coil in/out and room temperature difference.

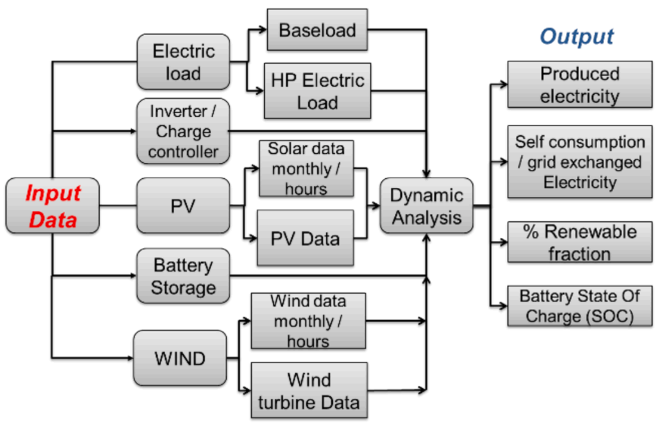

Fig. 4. PV/WT/BESS/Grid system modelling code workflow.

costs. The calculation model, developed in the EES environment, requires the following main input data

- **Nominal installed PV capacity and PV panels manufacturer's data** at Standard Test Conditions (STC) and the related coefficients.
- **Batteries nominal size $E_{battery}$** (capacity, kWh) and Dept of Discharge (DOD).
- **Balance Of System losses (BOS)** including PV reflectivity, mismatch, direct current losses, battery charge/discharge, inverter, and panel soiling.
- **Hourly solar radiation data and temperatures** (total G_{Ti} and beam G_{bi}) in the 12 monthly average representative days on the horizontal southern oriented plane for the selected location.
- **Hourly total electric load** in the 12 monthly average representative days, from the model of dynamic building heating/chilling, DHW and baseload outlined in the previous paragraph.
- **Wind Turbine** nominal size and characteristic curve.

2.1.3. Evaluation of solar and wind resource

The first step of the solar and wind resource assessment is the acquisition of datasets from historical measurements, which may be derived from measurements, as well as from suitable databases.

Regarding the solar resource, data were obtained from PVGIS [28], the European platform which provides the hourly solar radiation (G_{TI}). For the wind resource, data were collected from OpenWeather [29], an online platform providing forecasts and historical wind records. In this work, data from an area in southern Tuscany, covering the period from January 1st to December 31st, 2024, were used.

The calculation of the electricity production from the two sources relies on different sets of equations. For the PV system, manufacturer data are used, specifically the I–V curve and key parameters such as panel peak power, equation (11). It should be noted that many parameters, including module efficiency ($\eta_{PV,i}$) and BOS efficiency (η_{BOS}), and others vary with solar irradiance conditions. Therefore, the code evaluates these parameters on an hourly basis. The full set of equations applied is reported in the Supplementary Materials.

$$W_{PV,i} = G_{T,i} \bullet \frac{\eta_{PV,i}}{100} \bullet \frac{\eta_{BOS}}{100} \bullet A_{TOT,PV} \tag{11}$$

For the WT, a different approach was adopted. A statistical analysis of the wind dataset was carried out to define the Weibull fitting curve for each hour and month. The code then evaluates the expected value of each distribution by weighting wind speed with its relative frequency, thus constructing a theoretical available wind speed. Fig. 5 presents four examples of the automatically generated expected average hourly values of the wind distributions in four different representative seasonal months, along with one representative Weibull distribution per each month.

For the WT system, manufacturer data are used, specifically the characteristic power curve of the selected commercial machine showed in Fig. 6a (10 kW Ecolibri unit [30]). The turbine is 10 m high, with a rotor diameter of about 5.7 m, operating with cut-in, rated, and cut-off wind speeds of 3 m/s, 12 m/s, and 15 m/s, respectively. The WT power output varies with wind speed and is obtained by interpolating the characteristic curve, as expressed in equation (12), provided by the manufacturer and reported in Fig. 6b.

$$\begin{cases} if\ v_w < 3\ m/s \Rightarrow \quad W_{WT} = 0 \quad [W]; \\ if\ v_w \geq 3\ m/s \Rightarrow \quad W_{WT} = 12.16 - 13.41 v_w + 5.78 {v_w}^2 + 1.23 {v_w}^3 + 0.14 {v_w}^4 + 7.63x10^{-3} {v_w}^5 + 1.60x10^{-4} {v_w}^6 \quad [W] \end{cases} \tag{12}$$

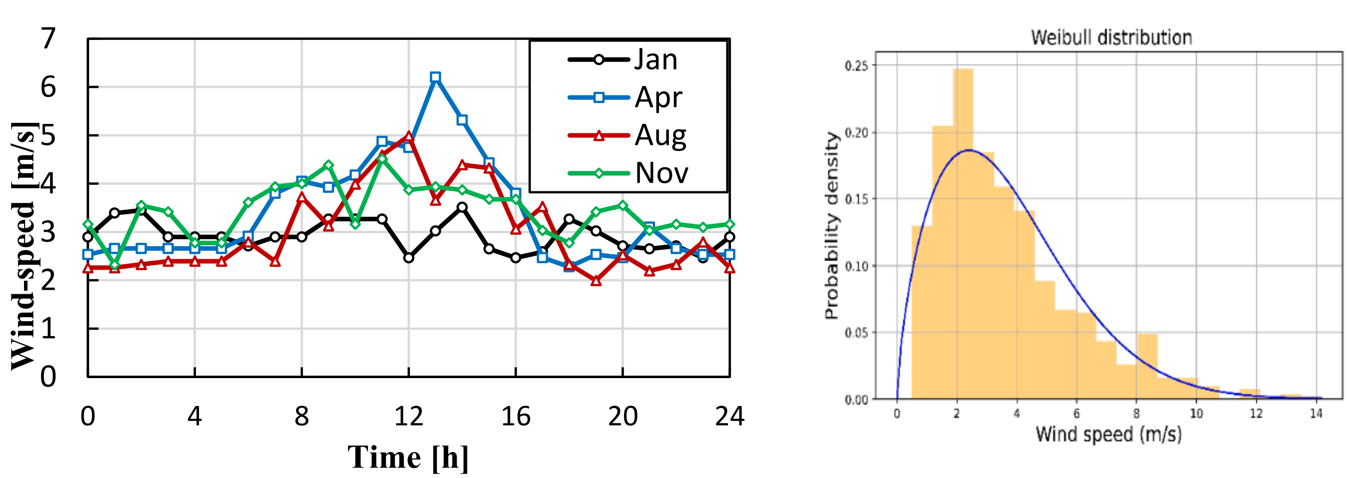

Fig. 5. Example of monthly data Weibull fit and daily representative wind elaborated data.

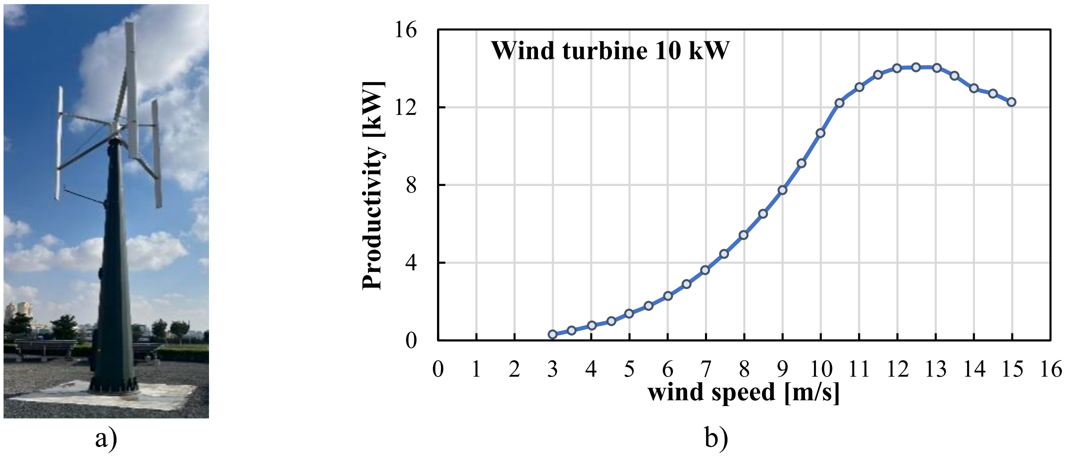

Fig. 6. Ecolibrì 10 kW wind turbine and characteristic curve [30].

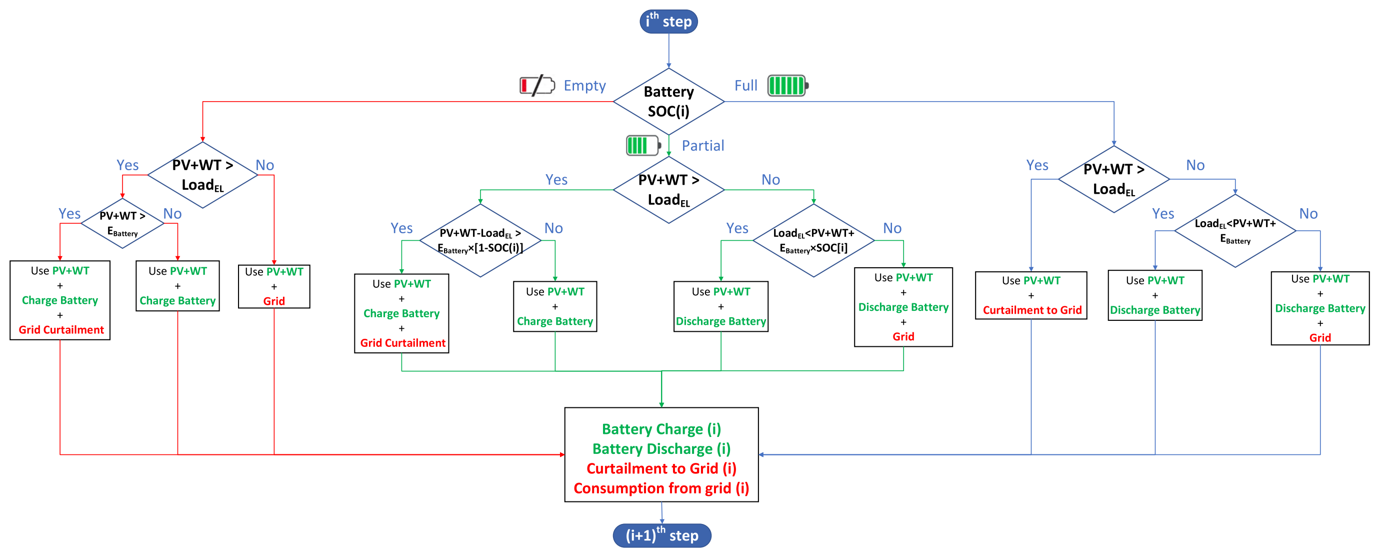

Fig. 7. Control logic of the Load – PV – battery – grid system.

2.1.4. Evaluation of battery charge and discharge dynamic

The hourly control logic of the PV–WT–BESS–Grid–Electric Load system is concisely illustrated in Fig. 7 and summarized below. It revolves around the three main conditions of battery State of Charge (SOC), expressed in the model as the hourly battery energy content (Battery[i]); $E_{battery}$ is the total battery capacity (kWh):

a) Battery partially charged;
b) Empty battery;
c) Full battery.

At every hour i of the selected monthly representative day, the overall electricity load $Load_{EL}[i]$ is compared to the sum of PV and WT production $W_{PV}[i] + W_{WT}[i]$. If this sum is sufficient, it directly feeds the load; otherwise, the battery support Battery[i] is called upon. Only if the current PV + WT production plus the residual battery charge is insufficient to meet the electricity load the grid supplies the remaining demand. In the case of excess PV and WT production, the surplus electricity charges the battery until it is full, with any additional surplus being fed back to the grid.

In the equations shown in the schematic, η_{ch}, η_{dis} and η_{inv} represent the BESS charge, discharge, and inverter efficiencies, respectively.

Since the calculation is based on the monthly representative day, the logic assumes periodicity of the battery SOC at midnight: Battery Charge [0] = Battery Charge[24]. Although, in reality, the SOC at midnight of each day depends on the charge/discharge history of the previous day, using the monthly representative day model, this assumption reasonably approximates the daily periodicity when considering all the days of the month. Furthermore, this approach is formally correct within the framework of the monthly representative day model.

Finally, the relevant parameters of the overall daily energy balances are calculated according to the equations reported in Table 2.

Table 2
Main daily energy balances of the grid connected pv/wt/bess system.

Equation	Unit	Description
$Load_{EL,day} = \sum_{i=1}^{N} Load_{EL,i}$	kWh	Total daily electric load
$E_{PV,day} = \sum_{i=1}^{N} W_{PV,i}$	kWh	Total daily electricity from PV
$E_{WT,day} = \sum_{i=1}^{N} W_{WT,i}$	kWh	Total daily electricity from WT
$EL_{grid,day} = \sum_{i=1}^{N} EL_{grid,i}$	kWh	Total daily electricity from the grid
$F_{r,day} = \frac{Load_{EL,day} - EL_{grid,day}}{Load_{EL,day}} \bullet 100\%$	%	Total daily renewable energy fraction

The battery charge/discharge efficiencies (η_{ch}, η_{dis}) were assumed at

96 %, as suggested in Zou et al., 2022 [31]. In addition, the inverter efficiency is also considered [32], and its modelling is reported in the Supplementary Materials.

2.2. Application of dynamic modelling to a representative case study and validation: building heating/chilling and baseload

The representative case study concerns a single-family house located in central Italy, in Tuscany, on a site characterized by 2,237 Degree Days. Originally built in 1990, the dwelling has recently undergone a deep refurbishment (2022–2023) that transformed it into a fully electric home, equipped with a reversible heat pump for both heating and cooling, and supported by a hybrid photovoltaic–battery system, while remaining connected to the national grid. The house extends over two floors, and its main dimensional and energy characteristics, before and after the renovation, are summarized in Table 3.

Two conditions have been examined. The first one represents the dwelling in its original state, with a relatively high overall thermal transmittance (U·A = 600 W/K), corresponding to an average U-value of 1.05 W/(m^2·K). The second represents the house after a moderate refurbishment, which reduced the transmittance to 320 W/K, with an average U-value lowered to 0.55 W/(m^2·K). The interventions that brought about this improvement are illustrated in Fig. 8 and include: insulation of the vertical walls (marked in orange), insulation of the attic and the ceilings beneath roof balconies (fuchsia and green areas, respectively), and replacement of doors and windows with high-performance units certified to a global transmittance of 1.2 W/(m^2·K), indicated in blue.

The second set of refurbishment measures involved the transition to fully electric utilities supported by PV:

- Reversible hydronic heat pump, 11.6 kW nominal capacity, providing heating, cooling, and DHW through a 380-litre storage tank.
- PV arrays installed on the south-east (4.8 kWp) and south-west (2 kWp) roof slopes, maximizing well-exposed surfaces, as shown in figure 8c).
- Battery storage consisting of four 5 kWh units, intentionally oversized thanks to incentives and in view of future PV expansion or integration of other renewables (e.g., wind).

Table 3
Main energy characteristics of the building pre and post refurbishment.

Data	Pre – refurbishment	Post – refurbishment
Net heated/cooled surface area [m^2]	177	177
Gross heated/cooled volume [m^3]	792	810
Envelope surface area [m^2]	573	581
Envelope surface/volume ratio	0.72	0.72
Overall energy consumption [kWh/(m^2 year)]	275 (F class)	103 (A4 class)
Renewable energy consumption [kWh/(m^2 year)]	32.30	89.00
CO_2 emissions [kg/(m^2 year)]	56	3
Summer solarized surface/net surface	0.11	0.04
Overall periodic transmittance Y_{IE} [W/(m^2 K)]	0.24	0.11
Overall averaged envelope heat transfer coefficient U including air changes [W/(m^2 K)]	1.05	0.55
Heating and DHW plant	LPG boiler (22 kW) + pellet stove (9 kW)	Air/water electric heat pump (11.6 kW)
PV powerplant nominal size [kWp]	0	6.80
Batteries overall size for electricity storage [kWh]	0	20

The Supplementary Material includes some images of the refurbishment works, as well as the electrical layout. Fig. 9 shows the manufacturer's COP curves (for heating, cooling, and DHW) of the commercial heat pump adopted in this case study, which can be considered a suitable representative unit.

In addition to the building, heat pump, PV, and battery specifications, the following inputs were considered:

- **Environmental data:** hourly solar radiation and outdoor temperature for each monthly representative day. Solar radiation data were obtained from JRC's PVGIS database (2004–2023 averages) [28], while temperature data were collected from a certified regional meteorological station and retrieved from the Tuscany Hydrologic Regional Database [33].
- **Baseload (BL) demand:** household electricity use for appliances and lighting, varying daily and seasonally, and strongly dependent on occupancy, location, and user habits. Since it is difficult to separate from the load of the reversible HP (heating, cooling, DHW), representative values were derived from ARERA's national database [34], aggregated by region and household nominal power. Data for 2022 were validated against utility bills from 2020 to 2022 (before refurbishment), showing that the 4.5–6 kW peak power category provides a reasonable estimation of BL for the case study. Some discrepancies were noted in July (due to holiday-related reductions in real load) and in late 2022 (when the HP was initially activated), but overall, the agreement between ARERA data and measured consumption confirmed the adequacy of this approach (Fig. 10 a).

The weighted average hourly baseload profiles for working days and weekends are shown in Fig. 10b, as an example of the estimation based on the ARERA database for different monthly representative days. These results are consistent with national Italian patterns reported by Torriti (2012) [35], Gallanti et al. (2012) [36], and MICENE Project data (2004) [37]. Alternative referenced baseload data can also be used in the model without losing generality.

The indoor set-point temperatures for winter and summer are shown in Fig. 11. In winter, the temperature is maintained at 20 °C from 7:00 to 22:00, with a progressive warm-up to 18 °C between 5:00 and 6:00 and a gradual cool-down between 22:00 and 23:00. During the night (0:00–4:00), the minimum temperature is set at 15 °C. In summer, the indoor comfort temperature is fixed at 26 °C, constant throughout the day. Based on these settings, the proposed model was used to dynamically calculate the hourly seasonal COP and electricity consumption of the reversible heat pump for space conditioning and DHW.

Fig. 12 illustrates an example of the calculated seasonal COP for both refurbished and non-refurbished cases. In summer, no significant differences were observed, while in winter the heat pump consistently achieved COP values above 3, even without refurbishment, thanks to its regulation adapted to ambient conditions.

2.3. Material thermodynamic rarity

This research also investigates the rarity of various materials within Energy System Equipment (ESE) streams using an exergy-based indicator named Thermodynamic Rarity (TR), as proposed by Valero Capilla et al., (2015) [38]. TR reflects the physical value of metals by considering the exergy requirements needed to extract and process elements from the Earth's crust into useful commodities or elements [39,40]. Exergy, defined as the maximum amount of work theoretically possible in bringing a resource into equilibrium with its environment through reversible processes [40], serves as the basis for this indicator. Valero Capilla et al., (2015) [38] established a reference point termed Thanatia, representing a hypothetical planet with exhausted resources, against which exergy costs for mining elements are calculated. The TR indicator combines two aspects: embodied exergy and exergy replacement costs [38]. Embodied exergy represents the exergy required to extract and

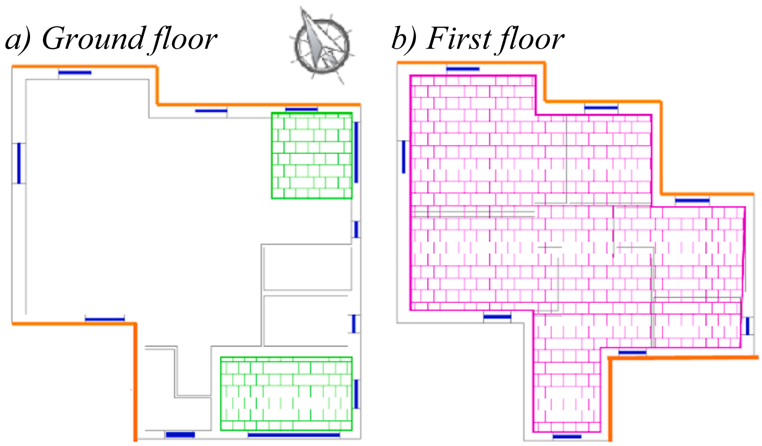

Fig. 8. Schematic of building plans, insulation interventions and roof with pv.

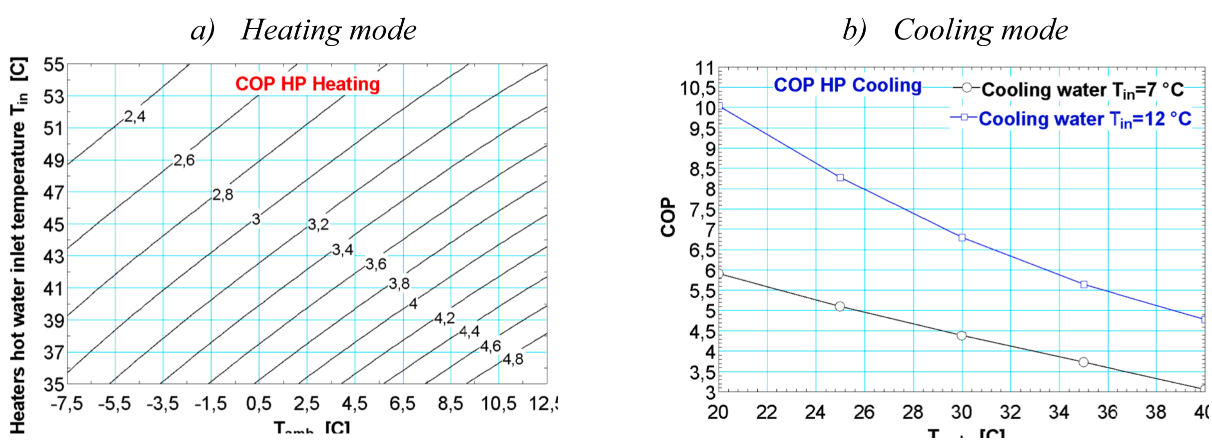

Fig. 9. Heat pump performance charts in heating (a) and cooling (b) mode.

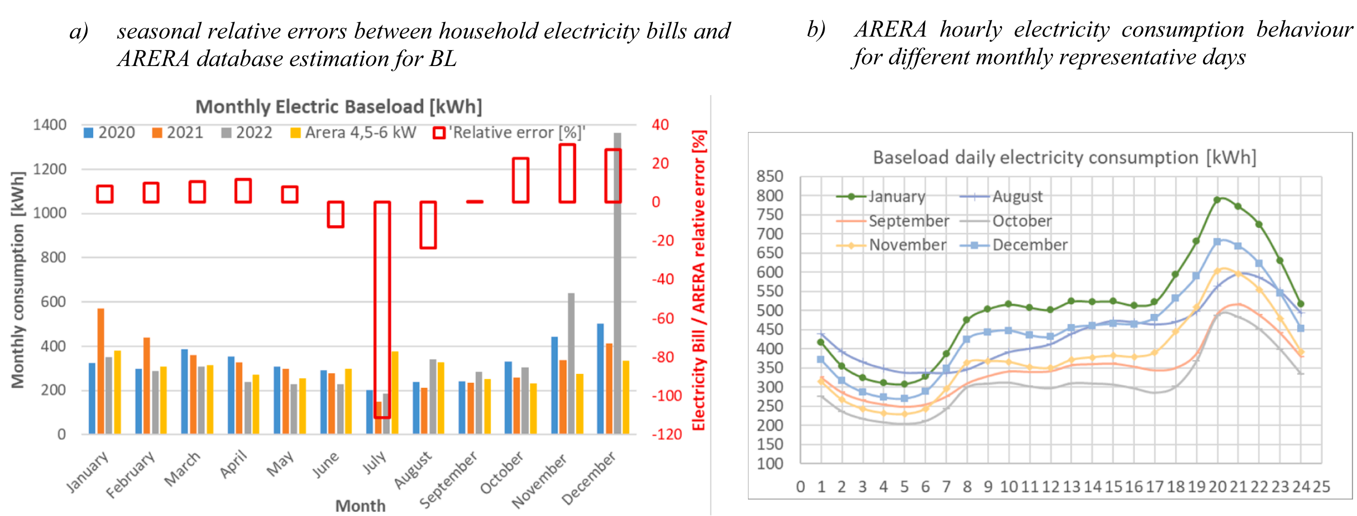

Fig. 10. Baseload household daily electricity consumption data, validation and elaboration from ARERA Database.

refine a mineral to produce a useful commodity, while exergy replacement costs encompass the total exergy needed to mine and concentrate a mineral deposit from average crustal concentration using current technologies [38]. Minerals are deemed valuable if they are scarce in nature [40] and/or costly to obtain due to extraction costs [41]. This methodology assigns values to minerals based on their relative abundance in the Earth's crust and the energy intensity required to refine them [42]. The TR indicator differs from other material assessment approaches [43], such as material footprints or ecological footprints, by focusing solely on the physical criticality of mineral resources through consistent exergy measurement [44,45]. In this instance, Energy System Equipment (ESE) comprises the devices outlined in preceding sections (HP,

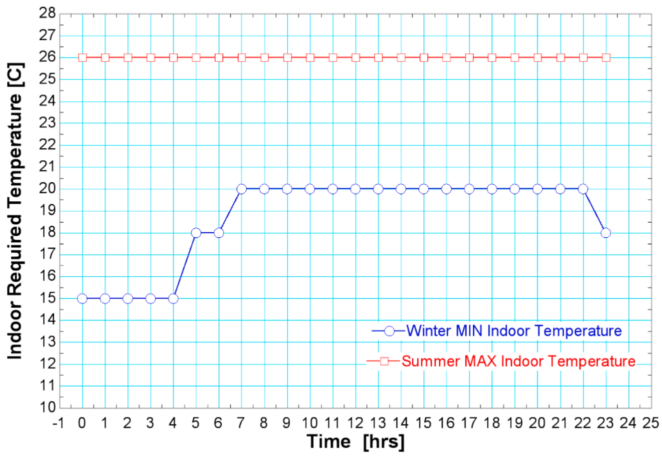

Fig. 11. Indoor set point temperature in winter and summer.

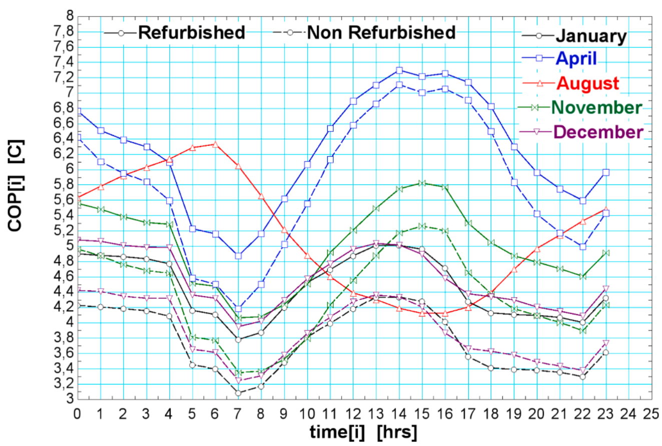

Fig. 12. Example of calculated seasonal Heatpump COP.

PV, WT, BESS). The methodology employed involved creating an inventory of the materials utilized in constructing these devices and subsequently characterizing each material at a chemical level. This facilitates the assessment of the Thermodynamic Rarity (TR) of each device.

This kind of analysis applied to buildings energy transition is not common in literature, which rather focuses on traditional sustainability indicators such as carbon and energy footprint. For this reason, it introduces the significant TR parameter as a complement of the traditional ones in the design and sustainability assessment of building energy transition, representing a relevant novelty point of the proposed paper.

3. Results

This section presents the results of the dynamic modelling and sustainability assessment in three main steps. First, the PV/BESS model is validated against experimental monitoring data and PVGIS simulations, highlighting seasonal patterns and system-specific anomalies (Section 3.1). Second, the validated model is applied to investigate the performance of different building configurations, focusing on optimal BESS sizing and the dynamic behaviour of PV/WT/BESS systems across seasons (Section 3.2). Finally, the analysis extends to the evaluation of material criticality, quantifying the rarity and supply risks associated with the main energy technologies considered (PV, WT, HP, and BESS) (Section 3.3).

3.1. Seasonal results and validation of the model

The dynamic modelling results of building electric utilities supplied by a PV/BESS/grid system are compared with data from the household energy monitoring system of the case study introduced in Chapter 3. The available dataset spans a 17-month monitoring period, starting from the commissioning of the PV/battery system in August 2023. This timeframe covers two complete autumn/winter cycles and approximately one and a half spring/summer periods. The reference case study does not include a wind turbine; thus, the renewable contribution derives entirely from the PV system.

Model outcomes were also validated against PVGIS results for the selected site, with particular attention to matching the PV/BESS performance parameters and BOS efficiency. This tuning is inherently uncertain, since PVGIS provides BOS losses as a lumped overall value. In line with PVGIS defaults, a 14 % BOS loss was adopted as the average reference for model validation. This comparison is especially relevant because the hourly solar radiation input to the model was sourced directly from PVGIS (SARAH2 database, CM SAF [46]).

The PV module specifications applied in the model are as follows:

- PV Panels nominal power size $W_{PAN} = 400$ W and surface area, $A_{TOT} = 2$ m^2;
- Nominal PV current $I_{mpp} = 7.88$ A, nominal PV voltage $V_{mpp} = 37.7$ V;
- Short Circuit PV current $I_{SC} = 8.35$ A, Open Circuit PV voltage $V_{OC} = 46.5$ V;
- Nominal Operating Cell temperature NOCT = 45 ± 2 °C;
- Coefficient of temperature/voltage at open circuit $\beta_{VOC} = -0.28$ %/°C;
- Coefficient of Short Circuit temperature $\alpha_{ISC} = +0.05$ %/°C;
- Coefficient of temperature/power $\gamma_{Pmax} = -0.35$ %/°C;
- Nominal efficiency of PV module ($\eta_{STC} = 19.9$ %).

The household energy monitoring system records data at 5-minute intervals. To reduce data volume while preserving representativeness, 15-minute intervals were adopted, with subsequent hourly averaging for each day.

Fig. 13 presents the validation of the developed model against the measured data from the case study. Specifically, Fig. 13a illustrates the comparison between measured data, model outputs, and PVGIS results. The light blue dots represent 15-minute measurements, while the orange dots indicate the corresponding hourly averages. The black line refers to the outcomes of the proposed model, whereas the green line shows PVGIS estimates. To further assess the quantitative accuracy, Fig. 13b reports the monthly total productivity obtained from three sources: measured data (orange), the developed model (black), and PVGIS (green).

The measured data from the household energy management system are organized into three categories:

- Inverter data – including PV input parameters such as time-resolved Maximum Power Point Tracker (MPPT) voltage and current, output power, inverter status, and temperature.
- Battery (BESS) data – including time-resolved charge and discharge power, energy charged/discharged, state of charge (SOC), and operational status.
- Grid meter data – recording the active power exchanged with the electrical grid.

For illustrative purposes, Fig. 13 presents only two months, representing the cases of minimum and maximum uncertainty in the results: April and August, respectively. For completeness, the data for other representative months are provided in the Supplementary Materials.

The results demonstrate that the model successfully captures the observed trends, confirming its representativeness with respect to the

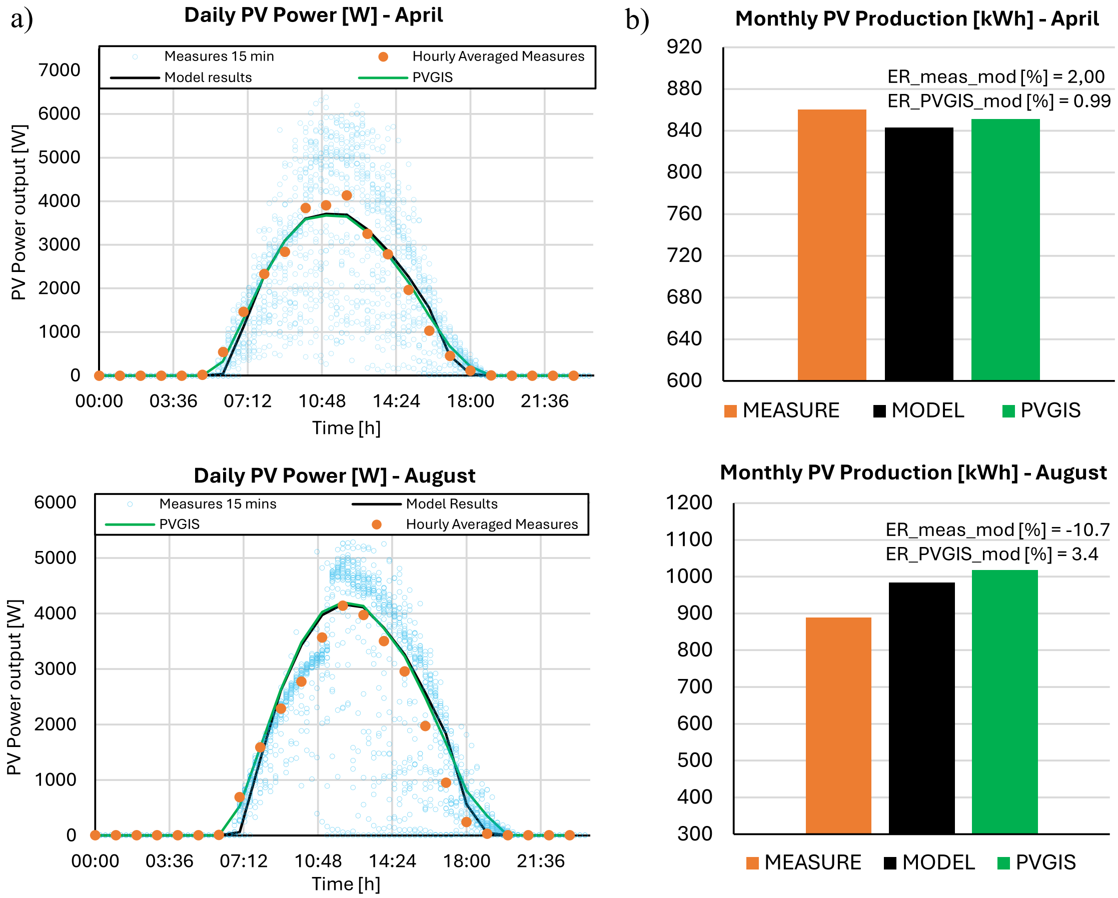

Fig. 13. Comparison of measured and calculated PV production dynamic data.

measured data. The comparison between hourly-averaged measured data and the dynamically calculated PV production shows, overall, good agreement. Slightly lower, yet still acceptable, agreement is observed during the summer months, particularly in August, where both the model and PVGIS tend to overestimate PV yield, with a relative error of approximately 9–10 % on total production. April shows a higher agreement. In general, the model overestimates PV production during summer, whereas it tends to underestimate it in winter and mid-season periods. Agreement with PVGIS is satisfactory across nearly all seasons, with relative errors on total production ranging between 1 % and 3.5 %.

The discrepancies between measured data and model results can be mainly attributed to two factors:

- Uncertainties in solar radiation data at the plant site during the measurement period: measured data correspond to 2023–2024, whereas model inputs are based on PVGIS data averaged over 2005–2023 (PVGIS, 2024 [28]).
- Uncertainties in Balance of System (BOS) losses, include mismatch, reflection, DC losses, soiling, and inverter parameters. The only directly measured parameter is the inverter efficiency, which shows satisfactory agreement with the model. Notably, during early and late daylight hours, the model closely matches measured data, whereas PVGIS tends to overestimate the PV production due to the use of a constant, lumped BOS efficiency value. This discrepancy is largely associated with reduced inverter efficiency at low DC input power, typical at the boundaries of daylight.

Minor discrepancies between the model and PVGIS outputs are primarily related to uncertainties in PV panel performance: the model uses manufacturer-specific data, while PVGIS assumes generic monocrystalline technology. Additionally, the lumped flat BOS loss in PVGIS introduces further differences. Nevertheless, since the radiation data for the model are sourced from PVGIS, the daily production curves show strong agreement, confirming the model's reliability.

The comparison with simulated data derived from the average monthly day model indicates that the observed discrepancies are attenuated but remain pronounced during periods characterized by predominantly clear-sky conditions (July and August), while they are largely negligible under conditions dominated by diffuse radiation (October-January). The morning performance of the PV2 string induces a daily energy deficit of 1–4 kWh on clear-sky days, more pronounced in summer, thereby accounting for the overestimation of summer energy yields reported by both the model and PVGIS. This anomaly is attributable to the PV system itself rather than to model limitations. An example is reported in Figs. 14 and 15, referred to two days of August 2024: clear sky (Fig. 14) and partially cloudy (Fig. 15). The working anomaly of PV2 in clear sky day is highlighted by the daily behaviour of PV2 input voltage drop in 4 – 5 morning hours, from sunrise to about 10 – 11 AM.

Considering the inter-annual variability of hourly PV generation, the PV/BESS model demonstrates a satisfactory level of accuracy and reliability for the purposes of the present study.

This is corroborated by the graphs in Figs. 16a and 16b, which report the Standard Deviation (STD) of hourly PV generation and the STD relative to the average hourly generation (STD Rel), respectively, as estimated by PVGIS for the site of the selected building over the period 2005–2023. Except for the less productive hours around sunrise and sunset, STD Rel ranges between 5 % and 20 % during central daylight

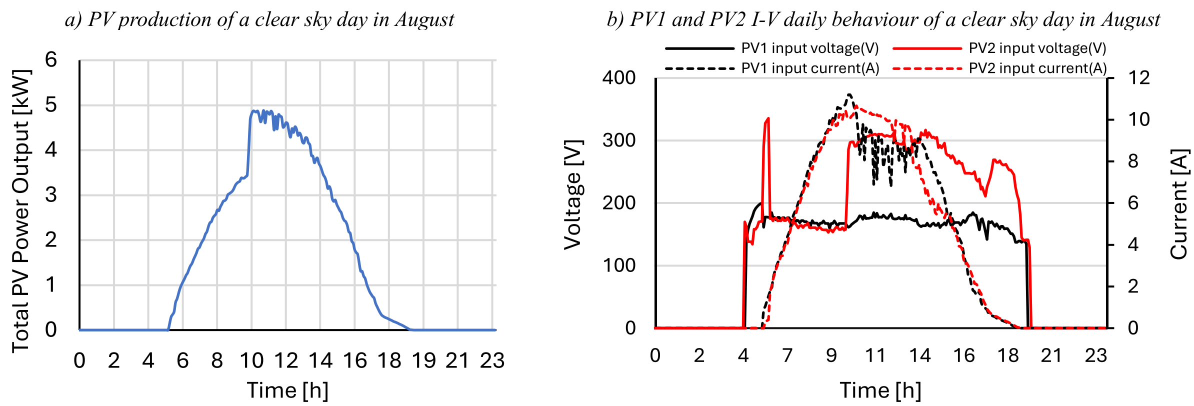

Fig. 14. Examples of daily productivity and I-V characteristics of the PV plant in a selected day with clear sky.

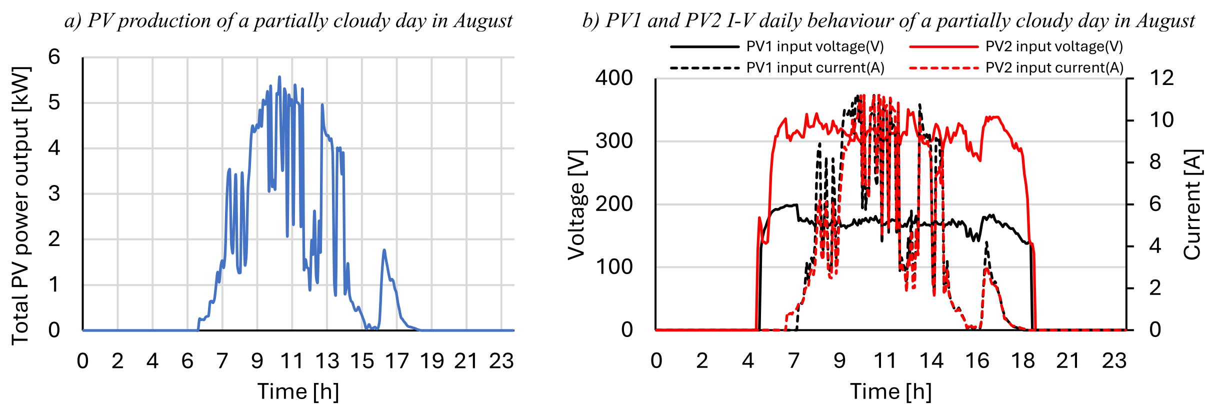

Fig. 15. Examples of daily productivity and I-V characteristics of the PV plant in different selected days with clear and partially cloudy sky.

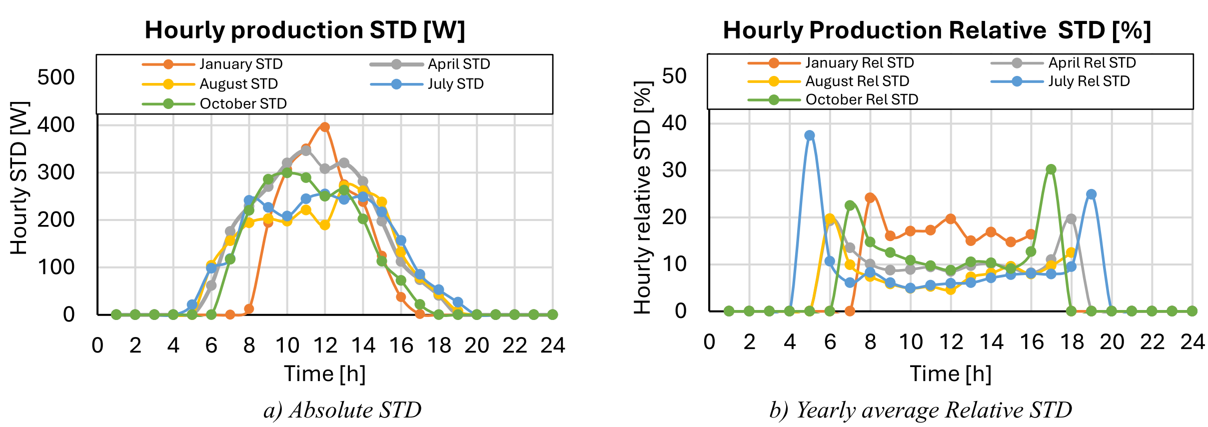

Fig. 16. Hourly STD of PV production along the years 2005 – 2023 for the selected site.

hours, with higher values in winter and lower values in summer due to the reduced stochastic component of solar radiation (e.g., less diffuse radiation in summer). Notwithstanding, the anomaly observed in the PV2 string under clear-sky conditions, the hourly deviations between model predictions and measured data generally remain within these bounds.

3.2. *results of dynamic modelling*

In line with the objective of this study, which also aims to evaluate the effectiveness of moderate interventions to enhance energy efficiency and renewable energy utilization in buildings, the following cases were analysed:

- non refurbished building with medium – high overall average heat transfer coefficient U = 1,05 W/(m^2 K), UA = 600 W/K with and without wind turbine;
- refurbished building with medium – low overall average heat transfer coefficient U = 0,55 W/(m^2 K), UA = 320 W/K, with and without wind turbine.

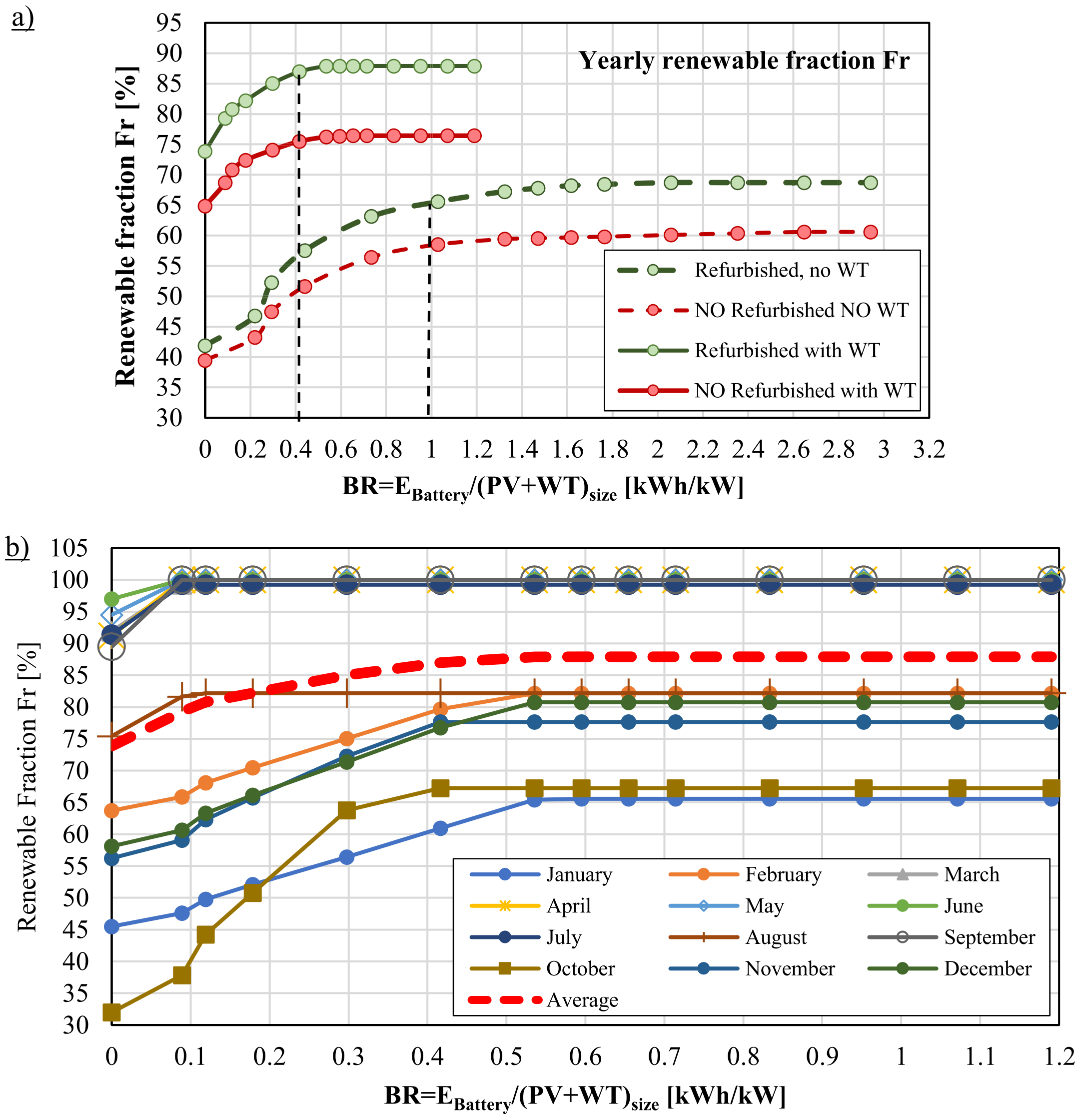

Fig. 17. Seasonal and average yearly behaviour of Fr vs BR, a) average yearly behaviour of Fr vs. BR; b) seasonal behaviour of Fr vs. BR; refurbished building, with WT.

3.2.1. *Optimal BESS sizing*

The dynamic simulation of the building/PV/WT/BESS system enabled the optimal sizing of the battery to maximize the renewable fraction (Fr) in meeting the building's electrical demand across all four analysed cases.

Fig. 17 a) illustrates the average annual behaviour of Fr as a function of the Battery Ratio (BR), defined as the ratio between the battery capacity and PV + WT nominal size: BR = $E_{battery}/PV_{size}$ when only PV is considered, and BR = $E_{battery}/(PV_{size} + WT_{size})$ when both PV and WT are included. As an example, Fig. 17 b) presents the seasonal behaviour of Fr for the refurbished building with WT, which is representative of the trends observed in all four cases.

The seasonal analysis highlights a higher sensitivity of Fr to BR from May to September, where increasing the BESS size results in nearly constant incremental gains over a broad range. Conversely, from October to February, the renewable fraction is maximized within a BR range of 0.4–0.6. The annual average behaviour, depicted in Fig. 18a, shows that Fr is similar across the four scenarios, indicating a substantial improvement (approximately 25 %) for BR values above 1 without WT, and above 0.41 with WT (black dashed vertical lines), beyond which further BESS size increases yield marginal gains (<10 %). This suggests that even a moderate addition of WT can significantly enhance Fr, taking advantage of the complementarity of solar and wind resources which allows the BESS size reduction.

The theoretical maximum achievable Fr is 68.7 % for the refurbished building with PV only, rising to 87.9 % with the inclusion of WT. For the non-refurbished building, the maximum Fr reaches 60.6 % with PV alone and 76.4 % with WT. Overall, adopting a BESS with BR = 1 enables Fr = 58.5 % in the non-refurbished building, increasing to 65.6 % with moderate refurbishment. Introducing a wind turbine further raises Fr to 76.4 % and 87.9 % without and with refurbishment, respectively, at a reasonable BR of 0.7 (corresponding to the same actual battery size in this study). Notably, deploying a BESS within the discussed size range significantly improves annual Fr, yielding 40–50 % in the refurbished building and 36–44 % in the non-refurbished building. Without any storage, the wind contribution alone increases Fr by approximately 10 percentage points.

3.2.2. *Dynamic behaviour of PV/WT/BESS system*

The dynamic performance of the PV/WT/BESS system is illustrated in Fig. 18 for the refurbished building scenario, with the non-refurbished building exhibiting similar trends. Four representative seasonal cases

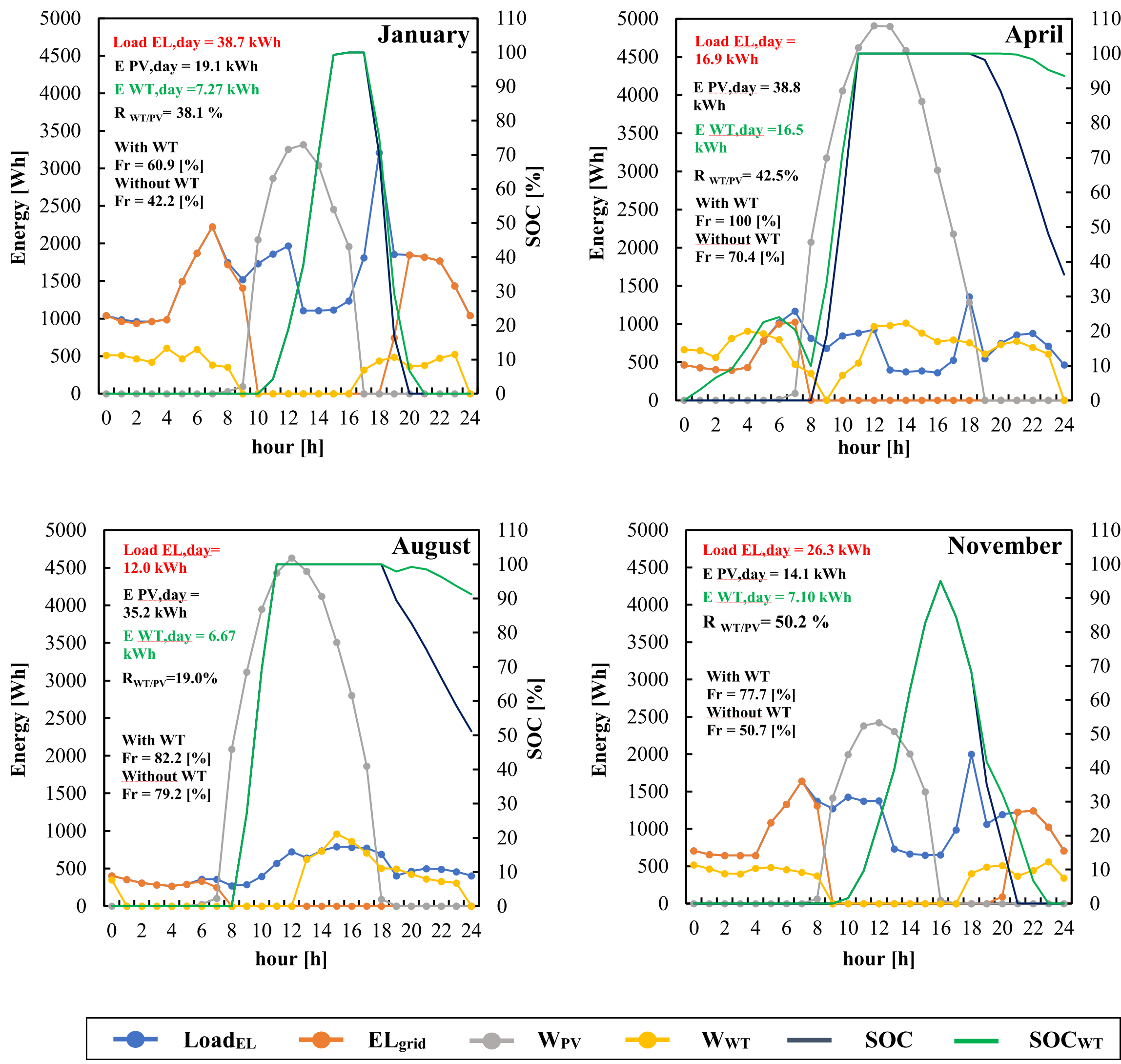

Fig. 18. Seasonal dynamic behavior of pv/wt/bess system in refurbished building in different months.

are presented, with the BESS sized at the optimal marginal values identified in the previous section, corresponding to BR = 1 and 0.41 for cases with and without WT, respectively. Generally, the contribution of the WT is more pronounced during winter and cloudy months, such as November, where wind-generated electricity significantly enhances the daily renewable fraction ($F_{r,day}$). As indicated by the graphs in Fig. 17, during winter and cloudy months, the ratio of daily wind to solar electricity generation $E_{WT,day}/E_{PV,day}$ ranges from 38 % to over 50 %. In spring, this ratio remains relatively high at approximately 40 %, whereas in summer it declines substantially, fluctuating between 15 % and 20 %. For the site in central Italy, both spring and summer exhibit high Fr values, reaching 100 % for refurbished buildings equipped with both PV and WT in April, and 70 % for those without WT. In August, the corresponding values are 82.9 % and 79 % respectively.

Across all scenarios, the integration of a properly sized Battery Energy Storage System (BESS) provides a substantial contribution to enhancing Fr, even during autumn and winter. This is evidenced by the observed BESS state of charge dynamics (SOC) and the extended periods of zero grid electricity consumption (EL_{grid} [i] = 0).

3.3. Rarity assessment of critical materials in building energy transition

The first step of the analysis delineates the chemical composition of materials utilized in energy devices, as depicted in Fig. 19. Wind Turbines (WT) and Heat Pumps (HP) predominantly consist of Iron (Fe), constituting 93 % and 80 % of their composition, respectively. Additionally, WT exhibits minor quantities of Aluminium (Al), Copper (Cu), and Silicon (Si) at 1.74 %, 1.09 %, and 2.26 %, respectively, with trace amounts of other elements encompassing the remaining share. In contrast, HP contains 19 % Copper (Cu) and trace amounts of other chemical constituents. Notably, Photovoltaic (PV) panels and Battery Energy Storage Systems (BESS) exhibit greater compositional variability. PV panels are predominantly composed of 67 % Silicon (Si) and 29 % Sodium (Na), with trace amounts of Aluminium (Al) and Copper (Cu) at 1.09 % and 2.67 %, respectively. Conversely, BESS comprises 11.2 % Aluminium (Al), 12.3 % Cobalt (Co), 42 % Copper (Cu), 17.5 % Iron (Fe), 3.08 % Lithium (Li), and 12 % Nickel (Ni).

The TR evaluation illustrated in Fig. 20 provides an overview of the total TRs of each device, along with the relative contributions of each chemical element.

A key observation is that the three technologies, such as WT, HP, and PV, exhibit differing impacts on material criticality. Specifically, the

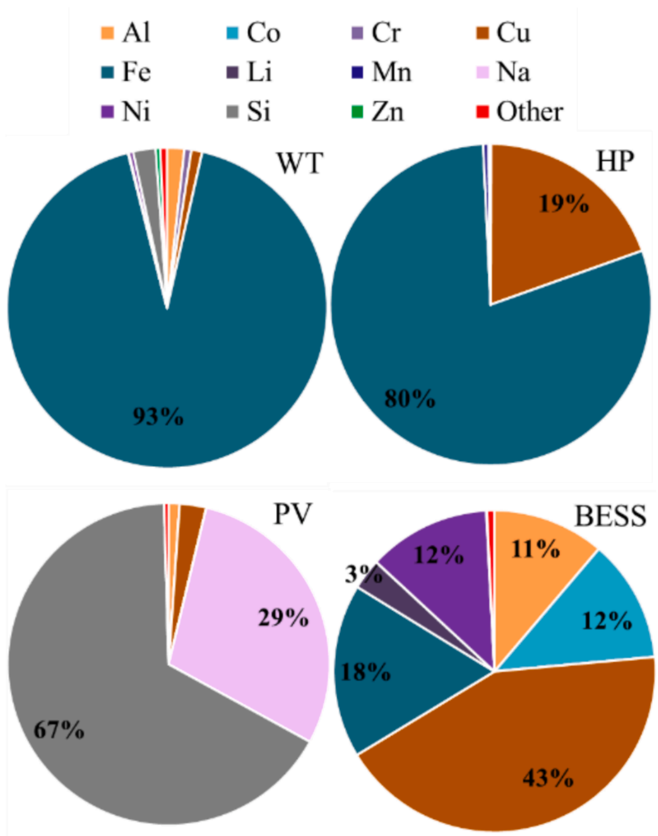

Fig. 19. Contribution analysis of chemical elements in each device.

highest TR impact is observed for WT, amounting to 68.2 GJ. Of this, approximately 50 % is attributed to Fe and 20 % to Al. Minor contributions come from other elements, such as Au (4.7 %), Cu (6.5 %), Mo (6.2 %), and Ni (5.4 %).

In contrast, the 12 kW HP has a significantly lower TR value of approximately 21.3 MJ, which is less than one-third of WT's impact. The impact of HP is primarily driven by Cu (72.0 %) and Fe (27.0 %). On the other hand, the 7 kW PV system has a TR value of 36 GJ, with 49 % of the impact attributable to Si and 24.7 % to Na. Additional contributions come from Cu (9.1 %), Ag (7.4 %), and Al (7.4 %).

The Battery Energy Storage System (BESS) plays a pivotal role in supporting variable renewable energy systems, such as WT and PV. Consequently, the TR contributions of these devices must also account for the impact of the BESS.

A parametric analysis reveals that for a 1 kWh BESS, the TR impact is significantly reduced to 5.22 GJ/kg, a substantially lower value compared to other technologies. However, when scaled to the preselected size of 7 kWh, the TR impact increases substantially, reaching 36.6 GJ/kg. This high impact is predominantly associated with Cobalt (Co) at 79.2 %, followed by Cu (8.7 %), Ni (5.2 %), and Al (4.5 %).

Finally, it is worth noting that while the TR impact decreases rapidly with a reduction in BESS size, there is a linear trend of increasing TR impact as the size of the BESS grows. This implies a significant rise in the criticality indicator when employing large-scale BESS units. For this reason, it may represent a valuable complement to the sustainable design of these systems, besides the traditional ones coming from LCA.

The parametric analysis indicates a significant reduction in impact, down to 5.22 GJ/kg for a 1 kWh size, a notably lower value compared to other technologies. However, it is noted that the storage function may not be adequately fulfilled. Additionally, as the impact decreases rapidly with a reduction in size, there is a linear trend for an increase in size, leading to a significant increase in this indicator when large BESS units are utilized.

4. Conclusions

The energy transition to full electric utilities of a suburban/country single household in middle Italy, grid connected and supported by a PV/WT/BESS system has been analysed by a dynamic energy modelling of academic origin. The level of building refurbishment has been intentionally kept moderate, to maintain the investigation within the area of affordability.

The analysis has been referred to a real case study of a single-family house equipped with PV only, against which the PV/BESS model has been validated and taken as representative of this kind of building. The model validation against real measured data from the PV/BESS management system of the household and with compliant PVGIS calculations revealed a satisfactory level of agreement, despite highlighting a working anomaly of the PV2 string of the real plant.

In the generalization of the results, four different cases have been analysed, e.g. non-refurbished and moderately refurbished buildings, with or without the addition of a WT. The existing high temperature heating system has been conserved and a high temperature hydronic seasonally reversable heat pump has been considered. The assessment of critical element involved in the building energy transition has been carried out though the thermodynamic rarity methodology. With renewable fraction Fr as objective function to cover the calculated electric load, the following relevant conclusions may be drawn:

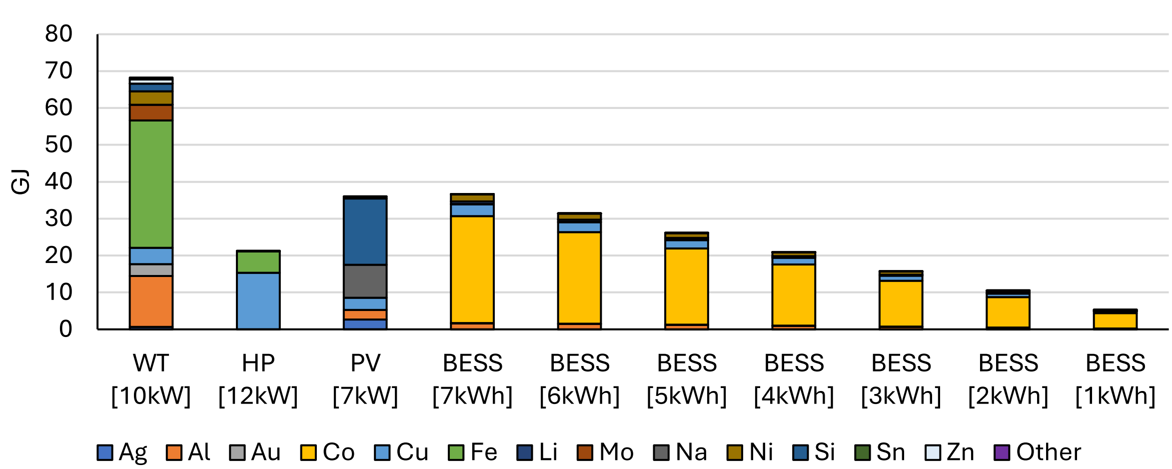

Fig. 20. Thermodynamic Rarity assessment.

- The marginal BR maximizing Fr is found at 1 with PV only and 0.4 with PV and WT, achieving a yearly Fr in the range 76 – 87 % with WT and 58 – 68 % without WT.
- The use of WT combined to PV and BESS allows significant flexibility in the possible options of various similar cases to achieve relevant values of Fr. The PV/WT/BESS size can be conveniently modulated and harmonized with the affordable building refurbishment level.
- The thermodynamic rarity assessment of the main energy transition critical elements has been carried out, highlighting the importance of flexible solutions in reducing their impact. Renewable variable energy systems require careful coupling with BESS because the latter have a very high TR, making it necessary to use the appropriate size for storage to avoid over-sizing.
- The developed dynamic model, validated against real data from a target building, has shown its effectiveness in the evaluation of PV/WT/BESS, reliably catching the influence of the main parameters of building envelope, heating/cooling equipment and renewable/storage system.
- The conservation of the existing radiators, which gives a fundamental contribution to the affordability in the shifting to heat pump, was demonstrated feasible and effective.

The future developments of the methodology and the related dynamic modelling will consider the economic analysis of the building and PV/WT/BESS, with minimum cost objective function to determine the optimal sizing. Elements of Artificial Intelligence (AI), available in the most recent versions of EES software, will be introduced in modelling and optimization procedures. Moreover, the combination with a Battery Electric Vehicle (BEV) will be considered in the framework of integrated mobility/building energy transition. Finally, the Life Cycle Assessment (LCA) of the whole system will be applied to evaluate the sustainability of the operation. The main impact categories, with special reference to the critical materials, will be combined to the Thermodynamic Rarity in the overall sustainability assessment of building energy transition.

CRediT authorship contribution statement

Claudio Zuffi: Writing – review & editing, Writing – original draft, Validation, Investigation, Formal analysis, Data curation. **Daniele Fiaschi:** Writing – review & editing, Writing – original draft, Validation, Supervision, Software, Methodology, Investigation, Formal analysis, Conceptualization.

Declaration of competing interest

The authors declare that they have no known competing financial interests or personal relationships that could have appeared to influence the work reported in this paper.

Appendix A. Supplementary data

Supplementary data to this article can be found online at https://doi.org/10.1016/j.ecmx.2026.101582.

Data availability

Data will be made available on request.

References

[1] IEA. Energy Statistics Data Browser. Paris: IEA; 2023. https://www.iea.org/data-and-statistics/data-tools/energy-statistics-data-browser.
[2] He Y, Liao N, Bi J, Guo L. Investment decision-making optimization of energy efficiency retrofit measures in multiple buildings under financing budgetary restraint. J Clean Prod 2019;215:1078–94. https://doi.org/10.1016/j.jclepro.2019.01.119.
[3] Bertoldi P, Economidou M, Palermo V, Boza-Kiss B, Todeschi V. How to finance energy renovation of residential buildings: Review of current and emerging financing instruments in the EU. Wiley Interdiscip Rev: Energy Environ 2021;10(1):e384.
[4] Aniello G, Bertsch V. Shaping the energy transition in the residential sector: Regulatory incentives for aligning household and system perspectives. Appl Energy 2023;333:120582. https://doi.org/10.1016/j.apenergy.2022.120582.
[5] Lovati M, Dallapiccola M, Adami J, Bonato P, Zhang X, Moser D. Design of a residential photovoltaic system: the impact of the demand profile and the normative framework. Renew Energy 2020;160:1458–67. https://doi.org/10.1016/j.renene.2020.07.153.
[6] Dermentzis G, Ochs F, Franzoi N. Four years monitoring of heat pump, solar thermal and PV system in two net-zero energy multi-family buildings. J Build Eng 2021;43:103199. https://doi.org/10.1016/j.jobe.2021.103199.
[7] Baraskar S, Günther D, Wapler J, Lämmle M. Analysis of the performance and operation of a photovoltaic-battery heat pump system based on field measurement data. Sol Energy Adv 2024;4:100047. https://doi.org/10.1016/j.seja.2023.100047.
[8] Terry N, Galvin R. How do heat demand and energy consumption change when households transition from gas boilers to heat pumps in the UK. Energ Buildings 2023;292:113183. https://doi.org/10.1016/j.enbuild.2023.113183.
[9] Vadiee A, Dodoo A, Jalilzadehazhari E. Heat supply comparison in a single-family house with radiator and floor heating systems. Buildings 2019;10(1):5. https://doi.org/10.3390/buildings10010005.
[10] European Union, Housing in Europe – 2024 edition, Eurostat; 2024, available at https://ec.europa.eu/eurostat/web/interactive-publications/housing-2024.
[11] Mulleriyawage UGK, Shen WX. Optimally sizing of battery energy storage capacity by operational optimization of residential PV-Battery systems: an Australian household case study. Renew Energy 2020;160:852–64. https://doi.org/10.1016/j.renene.2020.07.022.
[12] Chhugani B, Pärisch P, Helmling S, Giovannetti F. Comparison of PVT-heat pump systems with reference systems for the energy supply of a single-family house. Sol Energy Adv 2023;3:100031. https://doi.org/10.1016/j.seja.2022.100031.
[13] Olympios AV, Sapin P, Freeman J, Olkis C, Markides CN. Operational optimisation of an air-source heat pump system with thermal energy storage for domestic applications. Energ Conver Manage 2022;273:116426. https://doi.org/10.1016/j.enconman.2022.116426.
[14] Hessami MA. Designing a hybrid wind and solar energy supply system for a rural residential building. Int J Low-Carbon Technol 2006;1(2):112–26. https://doi.org/10.1093/ijlct/1.2.112.
[15] González A, Riba JR, Rius A. Optimal sizing of a hybrid grid-connected photovoltaic–wind–biomass power system. Sustainability 2015;7(9):12787–806. https://doi.org/10.3390/su70912787.
[16] Hajdidj MS, Bibi-Triki N, Didi F, Sreedhar T, Venkata N, Xu Y. Study and optimization of a renewable system of small power generation. EurJ Electrical Eng 2017;19(3–4):133–54. https://doi.org/10.3166/EJEE.19.133-154.
[17] Giallanza A, Porretto M, Puma GL, Marannano G. A sizing approach for stand-alone hybrid photovoltaic-wind-battery systems: a Sicilian case study. J Clean Prod 2018;199:817–30. https://doi.org/10.1016/j.jclepro.2018.07.223.
[18] Ramirez Camargo L, Nitsch F, Gruber K, Valdes J, Wuth J, Dorner W. Potential analysis of hybrid renewable energy systems for self-sufficient residential use in Germany and the Czech Republic. Energies 2019;12(21):4185. https://doi.org/10.3390/en12214185.
[19] Rehman S, Natrajan N, Mohandes M, Alhems LM, Himri Y, Allouhi A. Feasibility study of hybrid power systems for remote dwellings in Tamil Nadu, India. IEEE Access 2020;8:143881–90. https://doi.org/10.1109/ACCESS.2020.3014164.
[20] Drozd W, Kowalik M. Technical and cost comparison of selected technologies for energetic conversions of renewable energy sources. Arch Civ Eng 2021;67(1). https://doi.org/10.24425/ace.2021.136491.
[21] Nguyen TT, Boström T. Multiobjective optimization of a hybrid wind/solar battery energy system in the arctic. J Renew Energy 2021;2021(1):8829561. https://doi.org/10.1155/2021/8829561.
[22] McManus MC. Environmental consequences of the use of batteries in low carbon systems: the impact of battery production. Appl Energy 2012;93:288–95. https://doi.org/10.1016/j.apenergy.2011.12.062.
[23] Grandell L, Lehtilä A, Kivinen M, Koljonen T, Kihlman S, Lauri LS. Role of critical metals in the future markets of clean energy technologies. Renew Energy 2016;95:53–62. https://doi.org/10.1016/j.renene.2016.03.102.
[24] Huber ST, Steininger KW. Critical sustainability issues in the production of wind and solar electricity generation as well as storage facilities and possible solutions. J Clean Prod 2022;339:130720. https://doi.org/10.1016/j.jclepro.2022.130720.
[25] EN 442-2. Radiators and convectors – Part 2. Test methods and rating. Beuth Verlag, Berlin; 2014.
[26] UNI 10339, Air-conditioning systems - Classification, prescriptions and performance requirements for design and supply, AICARR (Associata REHVA – ASHRAE – IIF – UNI – CTI – ATI), 050101- 01, 2008, in Italian.
[27] Bearzi V. Handbook of Hydro Sanitary Installations, third Edition, EAN: 9788848125833, ISBN: 978-8848125833; 2013, in Italian.
[28] European Commission, PVGIS, Photovoltaic Geographical Information System, Last update: 01/03/2022, https://re.jrc.ec.europa.eu/pvg_tools/en/tools.html#SA.
[29] Meteostat, The Weather's Record Keeper, 2024, available on https://meteostat.net/en.
[30] Ecolibrì 10 kW-EW01 wind turbine, https://www.ecolibri.it/it/turbina-eolica/turbina-10kw/ [Website access on October 2025, in Italian].

[31] Zou B, Peng J, Li S, Li Y, Yan J, Yang H. Comparative study of the dynamic programming-based and rule-based operation strategies for grid-connected PV-battery systems of office buildings. Appl Energy 2022;305:117875. https://doi.org/10.1016/j.apenergy.2021.117875.
[32] Roberts JJ, Zevallos AAM, Cassula AM. Assessment of photovoltaic performance models for system simulation. Renew Sustain Energy Rev 2017;72:1104–23. https://doi.org/10.1016/j.rser.2016.10.022.
[33] Tuscany Regional Hydrological Service Portal of the Directorate of Soil Defense and Civil Protection; 2024, in Italian, available at https://www.sir.toscana.it/termometria-pub.
[34] Italian Regulatory Authority for Energy, Networks and Environment (ARERA), Analysis of domestic customer consumption; 2022, https://www.arera.it/dati-e-statistiche/dettaglio/analisi-dei-consumi-dei-clienti-domestici.
[35] Torriti J. Price-based demand side management: Assessing the impacts of time-of-use tariffs on residential electricity demand and peak shifting in Northern Italy. Energy 2012;44(1):576–83. https://doi.org/10.1016/j.energy.2012.05.043.
[36] Gallanti M, Grattieri W, Maggiore S, Marino A. Analisi ed evoluzione negli anni delle curve di carico dei clienti domestici. Energia Elettrica 2012;89(6):19–31.
[37] Franco Di Andrea AD. Misure dei Consumi di Energia in 110 abitazioni Italiane apparecchi di illuminazione (Progetto MICENE); 2004, in Italian.
[38] Valero Capilla A, Valero Delgado A. Thanatia: the destiny of the Earth's mineral resources: a cradle-to-cradle thermodynamic assessment. no Title 2015.
[39] Valero A, Valero A, Vieillard P. The thermodynamic properties of the upper continental crust: Exergy. Gibbs Free Energy and Enthalpy Energy 2012;41(1):121–7. https://doi.org/10.1016/j.energy.2011.06.012.
[40] Valero A, Valero A, Domínguez A. Exergy replacement cost of mineral resources. J Environ Accounting Manage 2013;1(2):147–58. https://doi.org/10.5890/JEAM.2013.05.004.
[41] Ortego A, Valero A, Valero A, Restrepo E. Vehicles and critical raw materials: a sustainability assessment using thermodynamic rarity. J Ind Ecol 2018;22(5):1005–15. https://doi.org/10.1111/jiec.12737.
[42] Ortego A, Valero A, Valero A, Iglesias M. Downcycling in automobile recycling process: a thermodynamic assessment. Resour Conserv Recycl 2018;136:24–32. https://doi.org/10.1016/j.resconrec.2018.04.006.
[43] Sen B, Onat NC, Kucukvar M, Tatari O. Material footprint of electric vehicles: a multiregional life cycle assessment. J Clean Prod 2019;209:1033–43. https://doi.org/10.1016/j.jclepro.2018.10.309.
[44] Wiedmann TO, Schandl H, Moran D. The footprint of using metals: new metrics of consumption and productivity. Environ Econ Policy Stud 2015;17:369–88. https://doi.org/10.1007/s10018-014-0085-y.
[45] Rees WE. Ecological footprints and appropriated carrying capacity: what urban economics leaves out. Environ Urban 1992;4(2):121–30. https://doi.org/10.1177/095624789200400212.
[46] CM SAF, The Satellite Application Facility on Climate Monitoring, EUMETSAT, 2020, https://www.cmsaf.eu/EN/Home/home_node.html.